

Sensitivity of stability charts with respect to modal parameter uncertainties for turning operations

David Hajdu* Tamas Insperger* Gabor Stepan*

* *Department of Applied Mechanics, Budapest University of Technology and Economics, Budapest, Hungary (e-mail: hajdu@mm.bme.hu, insperger@mm.bme.hu, stepan@mm.bme.hu).*

Abstract: Stability prediction of machining operations is often not reliable due to the inaccurate mechanical modeling. A major source of this inaccuracy is the uncertainties in the dynamic parameters of the machining center at different spindle speeds. The measured frequency response functions of the tool are usually loaded by noise and identification of the operational modal behavior based on static measurements is not straightforward. In this paper, the effect of small changes of the frequency response function on the stability of turning processes is analyzed using the semi-discretization method and the single-frequency solution.

Keywords: machine tool chatter, regenerative delay, frequency response function, sensitivity.

1. INTRODUCTION

Material removal by means of cutting is one of the most important components of manufacturing systems. Machine tool centers nowadays are capable of spindle speeds exceeding 50 000 rpm while simultaneously delivering tens of kilowatts of power to the cutting zone. Still, these features are often not utilized due to limitation caused by machine tool chatter. Prediction of the stability of a machining operation is therefore highly important for manufacturing systems.

In the 1960s, after the extensive work of Tobias (1965), Tlustý and Spacek (1954), the so-called regenerative effect became the most commonly accepted explanation for machine tool chatter. The phenomenon can be described by involving time delay in the model equations. The vibrations of the tool are copied onto the surface of the workpiece, which modifies the chip thickness and induces variation in the cutting-force acting on the tool one revolution later. This phenomenon can be described by delay-differential equations (DDEs).

Stability properties of the machining processes are depicted by the so-called stability lobe diagrams, which plot the maximum stable depths of cut versus the spindle speed. These diagrams provide a guide to the machinist to select the optimal technological parameters in order to achieve maximum material removal rate without chatter.

There are several limitations in the modeling of machine tool chatter. Most models in the literature consider linear systems, although nonlinear effects may also influence the stability properties (Dombovari et al., 2008). According to Munoa et al. (2013), the number of modes to be modeled is also an important factor. The approximation of the measured frequency response function (FRF) plays also an important role (Zhang et al., 2012). In this paper,

parameter sensitivity of the stability chart is analyzed for different modeling inaccuracies, such as mode omission or mode merging.

The structure of the article is as follows. In Section 2, the formulation of the frequency response function matrix in case of non-proportional damping is introduced. The stability analysis both in time domain (using the modal representation) and in frequency domain (using directly the measured FRF) are presented in Section 3. This provides two efficient ways to construct the stability charts. Some typical fitting inaccuracies are discussed in Section 5. First, the effect of neglected and merged modes is analyzed based on a two-degrees-of-freedom model. Then, the sensitivity of a stable island with respect to modal parameter inaccuracies are demonstrated. Finally, a case study is presented for different degrees-of-freedom approximation of a measured FRF. The results are concluded in Section 6.

2. DETERMINATION OF MODAL PARAMETERS

The modal behavior of the machine is usually determined from impact or shaking tests. Let us have the matrix differential equation of motion for a multiple-degrees-of-freedom system in the form

$$\mathbf{M}\ddot{\mathbf{x}}(t) + \mathbf{C}\dot{\mathbf{x}}(t) + \mathbf{K}\mathbf{x}(t) = \mathbf{f}(t), \quad (1)$$

where $\mathbf{x}(t) \in \mathbb{R}^n$ is the general coordinate vector, $\mathbf{M} \in \mathbb{R}^{n \times n}$ is the mass matrix, $\mathbf{C} \in \mathbb{R}^{n \times n}$ is the damping matrix, $\mathbf{K} \in \mathbb{R}^{n \times n}$ is the stiffness matrix, $\mathbf{f}(t) \in \mathbb{R}^n$ is the excitation vector and n is the number of degrees of freedom. Matrices \mathbf{M} , \mathbf{C} , and \mathbf{K} usually cannot be determined, but the modal parameters of the system can be approximated by different methods. Therefore the equations are defined in the modal space.

The system is proportionally damped if the damping matrix can be written as

$$\mathbf{C} = \alpha_M \mathbf{M} + \alpha_K \mathbf{K}, \quad (2)$$

where $\alpha_M \in \mathbb{R}$ and $\alpha_K \in \mathbb{R}$ are the proportional factors (Ewins, 2000). If the damping matrix can be represented in such a way, it guarantees that the mode shapes are real valued and identical to the eigenvectors of the undamped system. It is known that if a system is proportionally damped, then the frequency response function matrix $\mathbf{H}(\omega)$ can be defined as

$$H_{ij}(\omega) = \frac{X_i(\omega)}{F_j(\omega)} = \sum_{k=1}^n \frac{\phi_{ik}\phi_{jk}}{-\omega^2 + 2\zeta_k\omega_{n,k}\omega i + \omega_{n,k}^2}, \quad (3)$$

where ij represents the rows and columns of matrix $\mathbf{H}(\omega)$ respectively, $X_i(\omega) = \mathcal{F}(x_i(t))$, $F_i(\omega) = \mathcal{F}(f_i(t))$, and \mathcal{F} is the Fourier transform, furthermore $\omega_{n,k}$ is the natural angular frequency, ζ_k is the damping factor, $i = \sqrt{-1}$ is the complex unit, $\phi_{ik}\phi_{jk} = 1/m_k$, and m_k is the modal mass.

A system is called non-proportionally damped if (2) does not hold. In this case, the frequency response functions cannot be expressed according to (3), furthermore the mode shapes are complex and not identical to the eigenvectors of the undamped system. The equation of motion can be written in a first-order form

$$\hat{\mathbf{A}}\dot{\mathbf{v}}(t) + \hat{\mathbf{B}}\mathbf{v}(t) = \mathbf{f}_v(t), \quad (4)$$

where the state vector is $\mathbf{v}(t) = (\mathbf{x}(t) \dot{\mathbf{x}}(t))^T$ and

$$\hat{\mathbf{A}} = \begin{pmatrix} \mathbf{C} & \mathbf{M} \\ \mathbf{M} & \mathbf{0} \end{pmatrix}, \quad \hat{\mathbf{B}} = \begin{pmatrix} \mathbf{K} & \mathbf{0} \\ \mathbf{0} & -\mathbf{M} \end{pmatrix}, \quad \mathbf{f}_v(t) = \begin{pmatrix} \mathbf{f}(t) \\ \mathbf{0} \end{pmatrix}, \quad (5)$$

furthermore $\hat{\mathbf{A}} = \hat{\mathbf{A}}^T$ and $\hat{\mathbf{B}} = \hat{\mathbf{B}}^T$ (Ewins, 2000; Dombovari et al., 2012). The homogeneous part states an eigenvalue-eigenvector problem in the form

$$(\hat{\mathbf{A}}\lambda + \hat{\mathbf{B}})\mathbf{U} = \mathbf{0}, \quad (6)$$

where $\mathbf{U} \in \mathbb{C}^{2n}$ is the unnormalized (right) eigenvector. The eigenvalues can be determined from the frequency equation

$$\det(\hat{\mathbf{A}}\lambda + \hat{\mathbf{B}}) = 0, \quad (7)$$

where $\lambda_k = -\zeta_k\omega_{n,k} + \sqrt{1 - \zeta_k^2}\omega_{n,k}i$. The eigenvalues and eigenvectors form complex conjugate pairs if $\zeta_k < 1$.

Equation (4) can be transformed into the $2n$ -dimensional modal space by the transformation $\mathbf{q}(t) = \Psi\mathbf{v}(t)$, where $\mathbf{q}(t) \in \mathbb{C}^{2n}$ is the modal coordinate vector and $\Psi \in \mathbb{C}^{2n \times 2n}$ is the modal transformation matrix. If the complex eigenvectors \mathbf{U}_k are normalized according to the criteria

$$\psi_k = \frac{\mathbf{U}_k}{\sqrt{\mathbf{U}_k^T \hat{\mathbf{A}} \mathbf{U}_k}}, \quad (8)$$

then the modal transformation matrix can be written as

$$\Psi = (\psi_1 \bar{\psi}_1 \dots \psi_n \bar{\psi}_n). \quad (9)$$

Since $\Psi^T \hat{\mathbf{A}} \Psi = \mathbf{I}$ and $\Psi^T \hat{\mathbf{B}} \Psi = -\text{diag}(\lambda_k) = -\Lambda$, the equation finally forms

$$\dot{\mathbf{q}}(t) - \Lambda \mathbf{q}(t) = \Psi^T \mathbf{f}_v(t). \quad (10)$$

From the Fourier transform of (10), the elements of the FRF matrix $\mathbf{H}(\omega)$ consistently to (3) can be given as

$$H_{ij}(\omega) = \frac{X_i(\omega)}{F_j(\omega)} = \sum_{k=1}^n \left(\frac{\psi_{ik}\psi_{jk}}{\omega i - \lambda_k} + \frac{\bar{\psi}_{ik}\bar{\psi}_{jk}}{\omega i - \bar{\lambda}_k} \right). \quad (11)$$

Equations (11) and (3) are identical if the damping is proportional, then $\text{Re}\{\psi_{ik}\psi_{jk}\} = 0$. Using curve-fitting techniques, the modal parameters $\omega_{n,k}$, ζ_k , ψ_{ik} and ψ_{jk} can

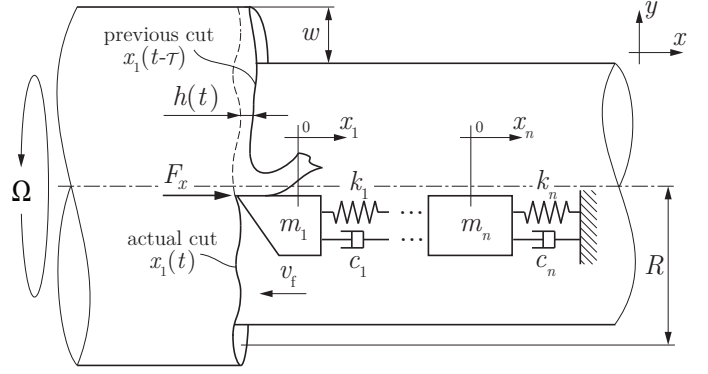


Fig. 1. Surface regeneration in an orthogonal process.

be fitted on the measured FRF. A well-known technique is the rational fraction polynomial method of Richardson and Formenti (1982), which can efficiently be used for high-degrees-of-freedom approximations, but there are many other linear or nonlinear fitting algorithms. In this paper, a nonlinear least squares method was used which is suitable for the fit of low-degrees-of-freedom models.

3. DYNAMICAL MODEL OF TURNING

The dynamical model of an orthogonal turning operation considering multiple modes in direction x is presented in Fig. 1. Note that vibrations in the y -direction does not affect the linear stability properties (Insperger et al., 2007). The cutting-force can be given as

$$F_x(t) = K_x w h^q(t), \quad (12)$$

where K_x is the cutting-force coefficient in the tangential direction x , w is the depth of cut, $h(t)$ is the instantaneous chip thickness and q is the cutting-force exponent. Due to the vibrations of the tool, the chip thickness is determined by the feed motion, the current tool position and the previous position of the tool one revolution ago. For constant spindle speeds, the time delay can be given explicitly as $\tau = 60/\Omega$, where Ω is the workpiece revolution given in rpm. The instantaneous chip thickness can be calculated as

$$h(t) = v_f \tau + x_1(t - \tau) - x_1(t), \quad (13)$$

where v_f is the feed velocity. Therefore the excitation vector $\mathbf{f}(t)$ can be given as

$$\mathbf{f}(t) = \begin{pmatrix} K_x w (v_f \tau + x_1(t - \tau) - x_1(t))^q \\ 0 \\ \vdots \\ 0 \end{pmatrix}. \quad (14)$$

The stability of the system can be analyzed by considering only the linearized system. The general solution can be given as $\mathbf{x}(t) = \mathbf{x}_p + \xi(t)$, where \mathbf{x}_p is related to the static deformation and $\xi(t)$ is a small perturbation around the equilibrium $\mathbf{x} \equiv \mathbf{x}_p$. After the linearization, the variational system is given by

$$\mathbf{M}\ddot{\xi}(t) + \mathbf{C}\dot{\xi}(t) + \mathbf{K}\xi(t) = \kappa(\xi(t - \tau) - \xi(t)), \quad (15)$$

and

$$\kappa = \begin{pmatrix} \kappa & 0 & \dots & 0 \\ 0 & 0 & \dots & 0 \\ \vdots & \vdots & \ddots & \vdots \\ 0 & 0 & \dots & 0 \end{pmatrix}, \quad \kappa = K_x w q (v_f \tau)^{q-1}, \quad (16)$$

where κ is the specific cutting-force coefficient. Note that κ is linearly proportional to the depth of cut w , which is an important machining parameter.

4. STABILITY ANALYSIS

Stability of machining processes can be analyzed either in frequency domain using directly the measured FRF or in time domain using the fitted modal parameters. The dynamic behavior of the tool tip determines the chip thickness, therefore the frequency response function associated with the tool tip is required, which can be expressed as

$$H_{11}(\omega) = \sum_{k=1}^n \left(\frac{\psi_{1k}^2}{\omega i - \lambda_k} + \frac{\bar{\psi}_{1k}^2}{\omega i - \bar{\lambda}_k} \right). \quad (17)$$

Consequently, only the parameters $\omega_{n,k}$, ζ_k and ψ_{1k} have to be fitted for the stability analysis.

4.1 Semi-discretization

If the modal parameters are fitted, the stable domains on the parameter space of the spindle speed Ω and the specific cutting-force coefficient κ can be determined by the semi-discretization method. According to the non-proportional formulation, equation (15) can be transformed into the modal space of the modal coordinates $\mathbf{q}(t)$ using the modal transformation $\boldsymbol{\xi}(t) = \boldsymbol{\Psi}\mathbf{q}(t)$, i.e.

$$\dot{\mathbf{q}}(t) - \mathbf{A}\mathbf{q}(t) = \boldsymbol{\Psi}^T \tilde{\boldsymbol{\kappa}} \boldsymbol{\Psi} (\mathbf{q}(t - \tau) - \mathbf{q}(t)), \quad (18)$$

and

$$\tilde{\boldsymbol{\kappa}} = \begin{pmatrix} \boldsymbol{\kappa} & \mathbf{0} \\ \mathbf{0} & \mathbf{0} \end{pmatrix}. \quad (19)$$

The state space equations can be introduced in the form

$$\dot{\mathbf{q}}(t) = \mathbf{A}\mathbf{q}(t) + \mathbf{B}u(t - \tau), \quad (20)$$

$$u(t) = \mathbf{D}\mathbf{q}(t), \quad (21)$$

where $\mathbf{A} = \mathbf{A} - \boldsymbol{\Psi}^T \tilde{\boldsymbol{\kappa}} \boldsymbol{\Psi}$. From a tip-to-tip measurement of the tool, only one row of matrix $\boldsymbol{\Psi}$ can be fitted. The matrices \mathbf{B} and \mathbf{D} can be reduced to vectors

$$\mathbf{B} = (\psi_{11} \ \bar{\psi}_{11} \ \cdots \ \psi_{1n} \ \bar{\psi}_{1n})^T \boldsymbol{\kappa}, \quad (22)$$

$$\mathbf{D} = (\psi_{11} \ \bar{\psi}_{11} \ \cdots \ \psi_{1n} \ \bar{\psi}_{1n}). \quad (23)$$

This shows that the frequency response function of the tool tip and the corresponding modal parameters are sufficient for the time-domain representation.

Stability of the system defined by (20)-(21) can be analyzed by the semi-discretization method according to Insperger and Stepan (2011). Note that here matrices \mathbf{A} , \mathbf{B} and \mathbf{D} have complex elements.

4.2 Frequency solution

The stability analysis can be performed directly in frequency domain using the measured FRF. This method can be applied directly to measured data without fitting.

The definition of the FRF matrix gives

$$\mathbf{H}(\omega)\mathbf{F}(\omega) = \boldsymbol{\xi}(\omega). \quad (24)$$

The Fourier transform of the parametric forcing $\mathbf{f}(t)$, which is the right hand side of (15) is

$$\mathbf{F}(\omega) = \boldsymbol{\kappa}(e^{i\omega\tau} - 1)\boldsymbol{\xi}(\omega). \quad (25)$$

Substitution of (24) into (25), and simplification yields

$$(\mathbf{I} - (e^{i\omega\tau} - 1)\boldsymbol{\kappa}\mathbf{H}(\omega))\mathbf{F}(\omega) = \mathbf{0}. \quad (26)$$

The existence of the nontrivial solution implies

$$\det(\mathbf{I} - (e^{i\omega\tau} - 1)\boldsymbol{\kappa}\mathbf{H}(\omega)) = 0, \quad (27)$$

which can be expressed as

$$1 - (e^{i\omega\tau} - 1)\boldsymbol{\kappa}H_{11}(\omega) = 0 \quad (28)$$

if only the first coordinate $x_1(t)$ is forced. If the inverse FRF is written as $H_{11}^{-1}(\omega) = \Lambda_{\text{Re}} + i\Lambda_{\text{Im}}$, then the analytic solution for all of the possible bifurcation curves can be given as

$$\Omega = \frac{30\omega}{\arctg\left(\frac{\Lambda_{\text{Re}}}{\Lambda_{\text{Im}}}\right) + j\pi}, \quad \kappa = -\frac{\Lambda_{\text{Re}}^2 + \Lambda_{\text{Im}}^2}{2\Lambda_{\text{Re}}}, \quad (29)$$

where $j = 0, 1, 2 \dots$ and $\omega \in [0, \infty)$. Note that the solution gives only the bifurcation curves, not directly the stable domains.

5. SENSITIVITY ANALYSIS

The real measured structure theoretically can only be described by an infinite dimensional (continuum) system. During curve fitting, however, only finite number of modes are fitted. In this section, the effect of imperfect mode fitting is analyzed.

5.1 Effect of neglected modes

In this subsection, the effect of neglected modes are analyzed. First an artificial FRF with proportional damping is generated and the stability charts are calculated using the frequency solution. The corresponding stability boundaries are denoted by black solid line and the stable domain is indicated by gray shading. Using a curve fitting technique, the original FRF was approximated by the FRF associated with a single-degree-of-freedom system, which is now also a proportionally damped model. These stability boundaries are denoted by red solid line.

Table 1 lists the original and approximated modal parameters while Fig. 2 presents the difference between the stability charts for four different cases. In each case, one mode is neglected during the fitting. For case a), the second mode at higher frequency with smaller amplitude is neglected. The estimated and exact boundaries show significant differences for high spindle speeds. It can be seen that the difference can go up to 100% near to 10 000 rpm, which means that the maximum stable depth of cut is doubled. For lower speeds, the stability chart is almost accurate. For case b), the neglected mode is larger, the difference is more significant.

Surprisingly, the chart is not that sensitive if the non-dominant mode is neglected at a lower frequency compared to the dominant mode. For cases c) and d), even if the neglected mode is apparently significant, the stable domain is practically the same for case c) and shows only a small change for case d). The reason is the following, when the neglected mode is located at lower frequency compared to the dominant mode then the corresponding bifurcation curves are likely to be located at negative cutting-force coefficients. In other words, based on (29), if $\Lambda_{\text{Re}} > 0$ then $\kappa < 0$ or $w < 0$ which is not relevant from the practical

Table 1. Modal parameters corresponding to the neglected modes (• are the fitted results).

| Case | ω_n [rad/s] | ξ [%] | ψ^2 [10 ⁻⁵ rad·s/kg] | $\tilde{\omega}_n$ [rad/s] | $\tilde{\xi}$ [%] | $\tilde{\psi}^2$ [10 ⁻⁵ rad·s/kg] |
|------|-----------------------|--------------|---|-------------------------------|----------------------|---|
| a) | 1000 | 5 | -5i | 1000.1 | 5.05 | -5.046i |
| | 2000 | 10 | -1i | × | × | × |
| b) | 1000 | 5 | -5i | 1000.2 | 5.17 | -5.142i |
| | 2000 | 10 | -3i | × | × | × |
| c) | 500 | 20 | -1i | × | × | × |
| | 1000 | 5 | -5i | 999.88 | 5.15 | -5.124i |
| d) | 500 | 20 | -5i | × | × | × |
| | 1000 | 5 | -5i | 999.25 | 5.96 | -5.734i |

point of view. This phenomenon can be seen in Fig. 3, whose subfigures correspond to Fig. 2 cases a) and c).

5.2 Effect of merged modes

In practice, the measured FRF contains many modes which are difficult to approximate properly. In many cases, some modes are so close to each other that they cannot be distinguished. In Fig. 4 some typical cases are listed, when two adjacent modes are approximated by only one mode. The exact and fitted modal parameters are given in table 2.

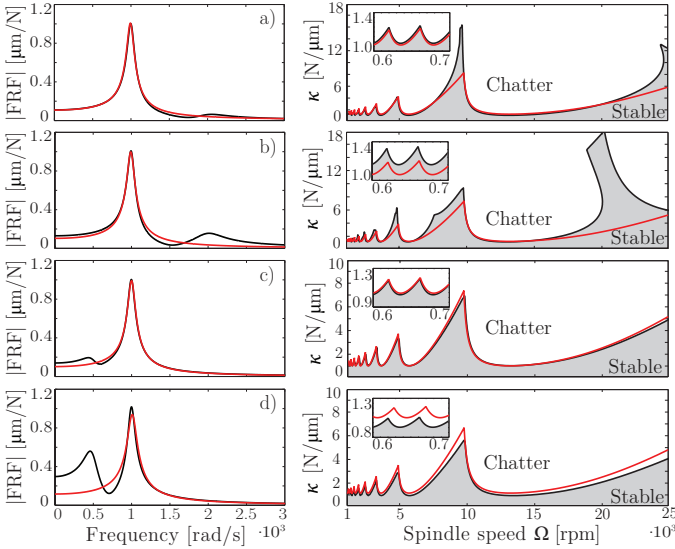


Fig. 2. Effect of neglected modes.

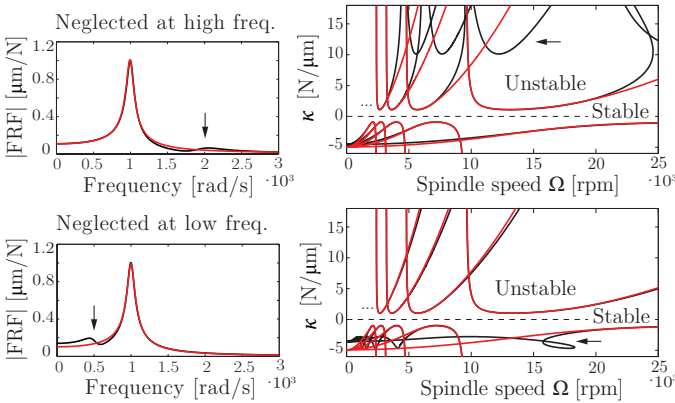


Fig. 3. Effect of neglected modes for negative cutting-force coefficients.

Table 2. Modal parameters corresponding to the merged modes (• are the fitted results).

| Case | ω_n [rad/s] | ξ [%] | ψ^2 [10 ⁵ rad·s/kg] | $\tilde{\omega}_n$ [rad/s] | $\tilde{\xi}$ [%] | $\tilde{\psi}^2$ [10 ⁵ rad·s/kg] |
|------|-----------------------|--------------|--|-------------------------------|----------------------|--|
| a) | 850 | 10 | -2i | 993.5 | 7.02 | -6.757i |
| | 1000 | 5 | -5i | × | × | × |
| b) | 1000 | 5 | -4i | 1042.6 | 7.46 | -8.926i |
| | 1080 | 4.5 | -4i | × | × | × |
| c) | 1000 | 5 | -4.5i | 1024.3 | 9.39 | -8.516i |
| | 1150 | 10 | -4i | × | × | × |

For case a), the neglected mode is located at lower frequency. The fitted mode does not describe properly the dominant mode, however, the chart practically does not change at higher spindle speeds. On the other hand, a larger shift in the stability boundaries can be seen at lower speeds. The effect of the neglected mode appears at the negative half plane, similarly as it is presented in Fig. 3.

When the two modes are very close and none of them is more dominant than the other (case b)), then the fitted stable domain slightly differs from the exact one. For high speeds, the wandering of the boundary is not significant, however a larger shift can be observed in the domains for lower spindle speeds.

Case c) is similar to case a), but here the non-dominant mode follows the dominant one. The change of the stability chart is more significant than in case a). As it can be seen, the boundaries are shifted at lower speeds too, and the difference is qualitatively larger for high speeds than in the other cases. The neglected mode has effect on the stability chart.

5.3 Stable islands in turning

The required time of the manufacturing process depends on the material removal rate, which linearly depends on the cutting speed, the feed rate and the depth of cut. The manufacturing time can be reduced, if any of those parameters are increased. The maximum revolution is limited by the capabilities of the machine tool, on the other hand, the depth of cut cannot be increased arbitrarily.

In some special cases, only for multiple-degrees-of-freedom systems, it can happen that a stable domain gets separated from a larger stable area (Sellmeier and Denkena, 2011;

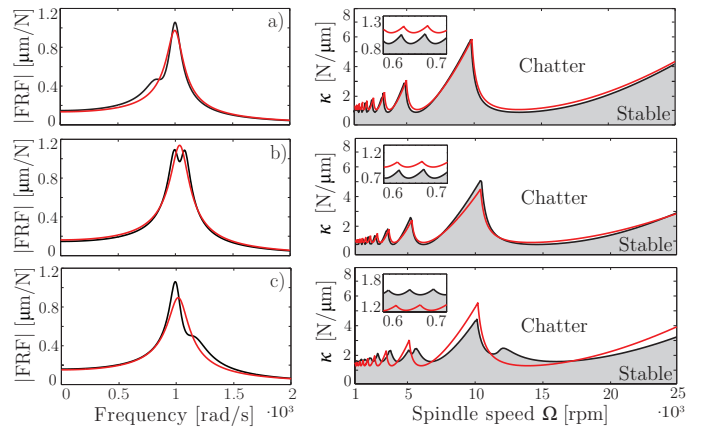


Fig. 4. Effect of merged modes.

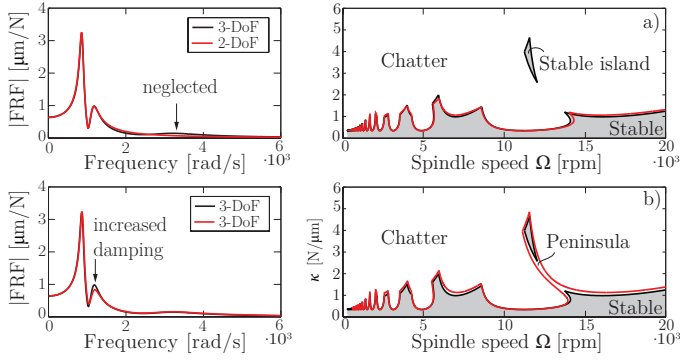


Fig. 5. Sensitivity of a stable island.

Table 3. Modal parameters for the three-degrees-of-freedom example (stable island).

| Mode | ω_n [$\frac{\text{rad}}{\text{s}}$] | ξ [%] | ψ^2 [$10^5 \frac{\text{rad} \cdot \text{s}}{\text{kg}}$] |
|------|---|--------------|--|
| 1 | 870 | 6.14 | -51.60-169.24i |
| 2 | 1150 | 10.60 | 60.66-118.14i |
| 3 | 3200 | 21.06 | -18.56-75.96i |

Zatarain and Dombovari, 2014). An example and its modal parameters are given in table 3 and the stability charts can be seen in Fig. 5.

The identification of these stable islands is a difficult task. Usually the islands are quite small and located at high spindle speeds, furthermore they can be really sensitive to the modal parameters. In Fig. 5 a), the third mode is neglected, since it does not seem to be significant compared to the others. Grey domains with black boundary indicates the originally stable chart, while red curve indicates the solution of the approximated system. The results show that the stable island disappears if the third mode is neglected, however the boundary of the stable domain does not change significantly.

In Fig. 5 b), the damping coefficient of the second mode was increased to 12.6% from 10.6%, and the third mode was not neglected. The stable island increases until it gets connected to the stable area and forms a peninsula. In real cases the fitted modal parameters always loaded by noise and error and the stable islands can easily get lost as it is demonstrated in Fig. 5.

5.4 A case study

In this subsection, a measured FRF obtained by an impact test for a milling tool is studied. In Fig. 6, the fitted model consists of 7-, 9-, 11- and 20 degrees of freedom respectively, where the non-proportional equations were used. For the 7-DoF model, the most dominant modes were approximated only. On the stability chart the grey domain indicates the theoretically exact stable domain obtained directly from the measured FRF using the frequency solution, while red curves indicate the result of the fitted functions. Stability boundaries for the fitted FRFs were also determined by the semi-discretization method in order to validate the results. As it can be seen for the lowest-degrees-of-freedom approximation, the stability chart for 10 000 – 25 000 rpm approximates the exact solution. For higher spindle speeds ($\Omega > 25\,000$ rpm), the difference in-

creases, but the approximation is still acceptable, and does not contain significant error. A stable island also appears if the chart is calculated using directly the measured FRF, but the first approximation does not show it.

The number of degrees of freedom was increased to improve the precision of fitting, and the FRF was approximated more accurately over the region 700-1200 Hz by taking into account two more modes. For lower speeds, the precision was improved, although for higher speeds, the error is much larger than in the case of the 7-DoF model, though the estimation of the FRF seems to be better.

The 11-DoF model provides a better result, although only two more modes were taken into account near to 882 Hz and 1318 Hz. Including new modes slightly change the modal parameters of the already fitted modes, but the approximation of the stability chart gets better. The stable island is still not discovered.

A 20-DoF approximation was prepared, where most of the non-dominant modes are taken into account. The measured FRF is very well covered by the fitted one, the difference is practically within line thickness. For low spindle speeds, the difference is negligible. The error between the stability boundaries slightly increases with the spindle speed. Overall, the 20-DoF model gives highly the best approximation and the stable island is also discovered.

6. CONCLUSION

Prediction of the stability of a machining operation requires information about the modal behavior of the machining center. The frequency response functions can only be determined by experiments, which is usually noisy and uncertain. Although there exists method which applies to measured FRFs directly, such as the single frequency solution or the multi-frequency solution (Altintas and Budak, 1995; Budak and Altintas, 1998; Bachrathy and Stepan, 2013), in many other techniques, fitted modal parameters shall be used. Though a fitted function is smoother and bases on a mechanical model, the results does not guarantee that the prediction of the stability chart is also better. When non-dominant modes are neglected or incorrectly fitted, the stability charts can significantly change. In this work, some typical fitting errors are considered and their effect is analyzed for a turning model.

It was shown, that if the neglected mode is located at lower frequency compared to the dominant mode, then the effect of the estimation is not significant. On the other hand, when the neglected mode is located at higher frequency compared to the dominant mode, then the estimated stability chart can qualitatively differ from the exact solution. It was also shown that the stability chart is also sensitive at higher spindle speeds, which is important in high speed machining. Even the estimation of the least significant modes can qualitatively change the stability boundaries.

The difference between the exact stability charts obtained by the frequency solution and the charts obtained using fitted models was demonstrated for a case study. In order to approximate properly the exact stability chart obtained directly from the measured FRF, high number of degrees of freedom must be considered, which can lead to difficulties.

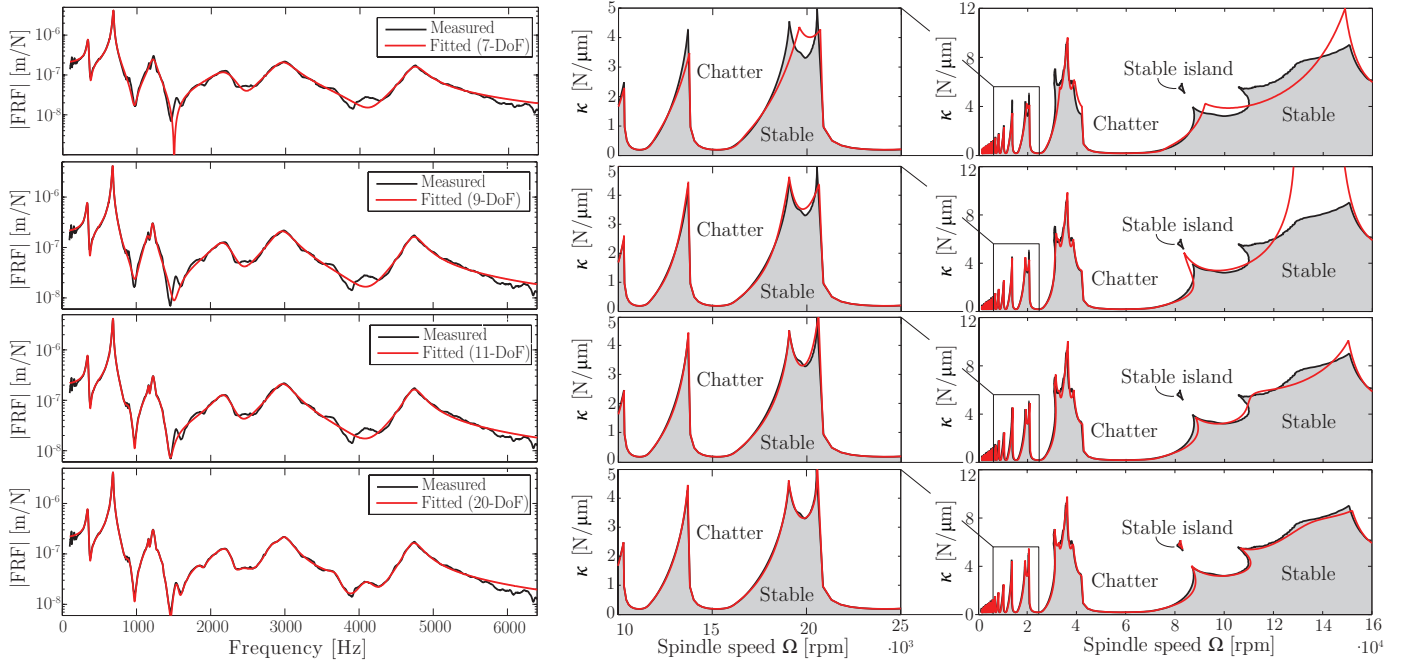


Fig. 6. The stability charts of the measured FRF. Solid black line indicates the direct solution obtained by the frequency solution, while solid red line shows the results of the fitted models.

For low spindle speeds, usually the precise approximation of the dominant modes is sufficient, however, for higher speeds, large variations can be observed which can hardly be predicted. The theoretically exact boundaries can be approximated sufficiently as more and more modes are taken into account. Still, even for the most precise fitting, the charts show slight sensitivity for high spindle speeds.

ACKNOWLEDGEMENTS

This work was supported by the Hungarian National Science Foundation under grant OTKA-K105433. The research leading to these results has received funding from the European Research Council under the European Unions Seventh Framework Programme (FP/2007-2013) / ERC Advanced Grant Agreement n. 340889.

REFERENCES

- Altintas, Y. and Budak, E. (1995). Analytical prediction of stability lobes in milling. *CIRP AnnManuf Techn*, 44, 357–362.
- Bachrathy, D. and Stepan, G. (2013). Improved prediction of stability lobes with extended multi frequency solution. *CIRP Annals - Manufacturing Technology*, 62, 411–414.
- Budak, E. and Altintas, Y. (1998). Analytical prediction of chatter stability in milling, part i: General formulation. *J Dyn SystT ASME*, 120, 22–30.
- Dombovari, Z., Munoa, J., and Stepan, G. (2012). General milling stability model for cylindrical tools. In *3rd CIRP Conference on Process Machine Interactions (3rd PMI)*, 90–97. Elsevier, Procedia CIRP 4.
- Dombovari, Z., Wilson, R.E., and Stepan, G. (2008). Estimates of the bistable region in metal cutting. *P Roy Soc AMath Phy*, 464, 3255–3271.
- Ewins, D.J. (2000). *Modal Testing, Theory, Practice, and Application*. Research Studies Press 2nd edition.
- Inserger, T. and Stepan, G. (2011). *Semi-discretization for time-delay systems*, volume 178. Springer, New York.
- Inserger, T., Stepan, G., and Turi, J. (2007). State-dependent delay in regenerative turning processes. *Non-linear Dynamics*, 47, 275–283.
- Munoa, J., Dombovari, Z., Mancisidor, I., Yang, Y., and Zatarain, M. (2013). Interaction between multiple modes in milling processes. *Machining Science and Technology*, 17, 165–180.
- Richardson, M.H. and Formenti, D.L. (1982). Parameter estimation from frequency response measurement using rational fraction polynomials. In *1st IMAC Conference*. Orlando, Florida.
- Sellmeier, V. and Denkena, B. (2011). Stable islands in the stability chart of milling processes due to unequal tooth pitch. *International Journal of Machine Tools and Manufacture*, 51, 152–164.
- Thusty, J. and Spacek, L. (1954). *Self-excited vibrations on machine tools*. Nakl. CSAV, Prague. in Czech.
- Tobias, S. (1965). *Machine-tool Vibration*. Blackie, Glasgow.
- Zatarain, M. and Dombovari, Z. (2014). Stability analysis of milling with irregular pitch tools. *Int. J. Dynam. Control*, 2, 26–34.
- Zhang, X.J., Xiong, C.H., Ding, Y., Feng, M.J., and Xiong, Y.L. (2012). Milling stability analysis with simultaneously considering the structural mode coupling effect and regenerative effect. *International Journal of Machine Tools and Manufacture*, 53, 127–140.